CMS Physics Analysis Summary

Contact: cms-pag-conveners-exotica@cern.ch 2011/08/23

Search for Extra Dimensions in the Diphoton Final State at the Large Hadron Collider

The CMS Collaboration

Abstract

A search for extra spatial dimensions in the diphoton final state has been carried out with the CMS detector at the LHC. Both resonant diphoton production via Randall–Sundrum graviton decay and non-resonant diphoton production via virtual Kaluza–Klein graviton exchange are considered. No excess of events above the standard model expectation is found using a data sample collected in proton-proton collisions at $\sqrt{s} = 7$ TeV and corresponding to an integrated luminosity of 1.1 fb^{-1}. New lower limits on the effective Planck scale in the range of 2.2–3.7 TeV at the 95% confidence level are set, providing the most restrictive bounds to date on the large extra dimensions model of Arkani-Hamed, Dimopoulos, and Dvali. Similarly, the most restrictive lower limits to date on the Randall–Sundrum graviton mass are set in the range of 0.76–1.73 TeV, for values of the coupling parameter between 0.01–0.10.

1 Introduction

The existence of extra spatial dimensions is an intriguing scenario that may solve the hierarchy problem [1] of the standard model (SM), the puzzling fact that the fundamental scale of gravity $M_{\rm Pl} \sim 10^{19}$ GeV is so much higher than the electroweak symmetry breaking scale $\sim 10^3$ GeV. With such a difference in scales, it is difficult to protect the Higgs boson mass from radiative corrections without a very high degree of fine-tuning.

The original proposal to use extra dimensions (ED) to solve the hierarchy problem was presented by Arkani-Hamed, Dimopoulos, and Dvali (ADD) [2, 3]. They posited a scenario wherein the SM is constrained to the common 3+1 space-time dimensions (brane), while gravity is free to propagate through the entire multidimensional space (bulk). Thus, the gravitational flux in 3+1 dimensions is effectively diluted by virtue of the multidimensional Gauss's Law. The fundamental Planck scale $M_{\rm D}$ is therefore related to the apparent scale $M_{\rm Pl}$ according to the formula

$$M_{\rm D}^{n_{\rm ED}+2} = \frac{M_{\rm Pl}^2}{r^{n_{\rm ED}}}, \tag{1}$$

where r and $n_{\rm ED}$ are the size and number of the EDs, respectively.

Another model of EDs that solves the hierarchy problem is due to Randall and Sundrum (RS) [4]. In this scenario—as in the ADD scenario—the SM is constrained to the brane while the graviton may propagate throughout the bulk. However, in the RS scenario, the observed hierarchy is due instead to the warped geometry of the EDs, rather than their physical size. In this paper, we consider the RS1 model, where only one finite ED exists separating two branes, one at each end. The geometry of the bulk is based on a slice of AdS_5 space with a length $\pi r_{\rm c}$, where $r_{\rm c}$ is the compactification radius. The full metric is given by

$$ds^2 = e^{-kr_{\rm c}y}\eta_{\mu\nu}\,dx^\mu dx^\nu - r_{\rm c}^2 dy^2, \tag{2}$$

where Greek indices run over 4-dimensional space-time, $\eta_{\mu\nu}$ is the Minkowski metric tensor, and $0 \le y \le \pi$ is the coordinate along the single ED of radius $r_{\rm c}$. The value of k specifies the curvature scale (or "warp factor") and relates the fundamental Planck scale on one brane to the apparent scale on the other by

$$M_{\rm D} = M_{\rm Pl}e^{-kr_c\pi}. \tag{3}$$

Therefore, TeV scales naturally solve the hierarchy problem in this model when $kr_c \sim 10 - 11$.

In the RS scenario, gravitons appear as a well-separated tower of Kaluza–Klein (KK) excitations with masses and widths determined by the parameters of the RS1 model. One convenient choice of parameterization is the mass of the first graviton excitation mode M_1 and the dimensionless warp factor

$$\tilde{k} \equiv \frac{k}{M_{\rm Pl}}, \tag{4}$$

which defines the strength of coupling of the graviton to the SM fields. Precision electroweak data constrains $\tilde{k} \gtrsim 0.01$, while perturbativity requirements limit $\tilde{k} \lesssim 0.1$. The excited gravitons can decay into two photons, but decays to fermions are suppressed relative to photons because the graviton is spin–2, and so fermions cannot be produced in the s wave.

Phenomenologically, the ADD scenario also results in s-channel production of massive KK graviton states, which can decay into two photons. However, unlike the RS model, the wavefunction of the KK gravitons must satisfy periodic boundary conditions, resulting in discrete energy levels with modal spacing of the order of the inverse ED size, from 1 meV to 100 MeV.

This results in an apparent continuum spectrum of diphotons, rather than distinct resonances, at high diphoton invariant mass $M_{\gamma\gamma}$.

Summing over all KK modes in the ADD scenario results in a divergence in the cross section, so an ultraviolet (UV) cutoff scale M_s is imposed. This cutoff scale is related to—but potentially different from—the fundamental Planck scale M_D. The precise relationship depends on the UV completion of the effective theory. The effects of virtual-graviton production on the cross section are parameterized by the single variable $\eta_G = \mathcal{F}/M_S^4$, where $\mathcal{F}$ is an order-unity dimensionless parameter, for which several conventional assumptions exist:

$$\mathcal{F} = 1 \quad \text{(Giudice, Rattazzi, and Wells, GRW [5])}, \tag{5}$$

$$\mathcal{F} = \begin{cases} \log\left(\frac{M_S^2}{\hat{s}}\right) & \text{if } n_{ED} = 2 \\ \frac{2}{(n_{ED}-2)} & \text{if } n_{ED} > 2 \end{cases} \quad \text{(Han, Lykken, and Zhang, HLZ [6])}, \tag{6}$$

$$\mathcal{F} = \pm\frac{2}{\pi} \quad \text{(Hewett [7])}, \tag{7}$$

where $\sqrt{\hat{s}}$ is the center-of-mass energy of the hard parton-parton collision. We note that the HLZ convention (uniquely among the three) contains an explicit dependence on the number of EDs.

Searches for EDs via virtual-graviton effects in the ADD model have been conducted at HERA, LEP, and the Tevatron (Refs. [8, 9] contain recent reviews of these searches). The most stringent previously published limits on M_S for $n_{ED} \geq 3$ come from the previous measurement in this channel at the Compact Muon Solenoid (CMS) experiment [10]. For $n_{ED} = 2$, the D0 measurements in the dijet [11] and diphoton plus dielectron [12] channels are more restrictive. The most restrictive previous search for RS gravitons was also conducted at the D0 experiment [13]. They present a search in the dielectron and diphoton channel, excluding graviton masses $M_1 < 0.56$ (1.05) TeV for $\tilde{k} = 0.01$ (0.10).

In this paper, we present a search for both non-resonant and resonant diphoton production, in the ADD and RS models, respectively. We use a data sample corresponding to an integrated luminosity of 1.1 fb^{-1}, collected in pp collisions at $\sqrt{s} = 7$ TeV at the CERN Large Hadron Collider (LHC) with the CMS detector.

2 The CMS Detector

CMS is a general-purpose detector designed to study proton collisions at the LHC and is described in detail in Ref. [14]. The detector consists of an all-silicon tracker, an electromagnetic calorimeter (ECAL), and a hadronic sampling calorimeter (HCAL), all contained inside a large-bore 3.8 T superconducting solenoid. In the central region, the tracker consists of three layers of silicon pixel detectors, followed by ten layers of single- and double-sided silicon-strip detectors. The calorimeter towers are projective and finely segmented, with $\Delta\eta \approx \Delta\phi \approx 0.087$ in the central region. Moreover, each tower consists of a five-by-five transverse grid of ECAL crystals ($\Delta\eta \approx \Delta\phi \approx 0.0174$), allowing precise reconstruction of the e/γ position and energy. Here, the pseudorapidity η is defined as $-\ln(\tan\frac{\theta}{2})$, where θ is the polar angle with respect to the direction of the counterclockwise beam, and ϕ is the azimuthal angle. Beyond the solenoid there are four layers of muon detectors, which are interspersed throughout the steel return yoke of the magnet. The instantaneous luminosity is measured with a relative uncertainty of 4.5% using information from forward hadronic calorimeters [15].

The CMS trigger system consists of two levels. The first level (L1), composed of custom hardware, uses information from the calorimeters and muon detectors to select the most interesting events for more refined selection and analysis at a rate of up to 80 kHz. The software-based High Level Trigger further decreases the rate to a maximum of ∼300 Hz for data storage. Events for the control samples used in this analysis were collected through a single-photon trigger, where the photon was required to have a transverse energy $E_{\mathrm{T}} \equiv E \sin\theta$ of at least 30, 75, 90, or 125 GeV, depending on the data collection period. Events in the signal sample were collected through a double photon trigger, where each photon was required to have $E_{\mathrm{T}} > 33$ GeV, $E_{\mathrm{T}} > 50$ GeV, or $E_{\mathrm{T}} > 60$ GeV depending on the instantaneous luminosity.

3 Event Reconstruction and Selection

We require that an event be consistent with a pp collision and have at least one well-reconstructed primary vertex [16]. We then reconstruct photons with $E_{\mathrm{T}} > 70$ GeV in the ECAL barrel fiducial region ($|\eta| < 1.44$) by clustering electromagnetic energy depositions in the ECAL. The ECAL clusters are five crystals wide in η and a variable length in ϕ to capture associated electromagnetic energy from possible photon conversions in the tracker. If hits are present in the pixel detector consistent with an electron track whose momentum and location is compatible to the energy and location of the ECAL cluster, then the cluster is rejected as a photon candidate.

Hadronic jets can be misidentified as photons when their leading hadron is a hard π^0 or η. We reduce the misidentification rate by placing the following restrictions on the isolation of the cluster: (i) the hadronic energy within $\Delta R < 0.15$ of the cluster must be less than 5% of its electromagnetic energy, where $\Delta R \equiv \sqrt{\Delta\phi^2 + \Delta\eta^2} \equiv \sqrt{(\phi - \phi_\gamma)^2 + (\eta - \eta_\gamma)^2}$; (ii) the ΣE_{T} of HCAL energy surrounding the cluster within $0.15 < \Delta R < 0.40$ must be less than $2.2\,\mathrm{GeV} + 0.0025 E_{\mathrm{T}}^{\gamma}$; (iii) the scalar sum of the transverse momentum of tracks, Σp_{T}, associated with the primary event vertex surrounding the cluster within a hollow cone of $0.04 < \Delta R < 0.40$ must be less than $2.0\,\mathrm{GeV} + 0.001 E_{\mathrm{T}}^{\gamma}$ (a rectangular strip of $\Delta\eta \times \Delta\phi = 0.015 \times 0.400$ at the front face of the ECAL is excluded from the track p_{T} summation to allow for photons that convert into $\mathrm{e}^+\mathrm{e}^-$ pairs); and (iv) the ΣE_{T} of ECAL energy surrounding the cluster within $0.06 < \Delta R < 0.40$ (and excluding a strip of $\Delta\eta \times \Delta\phi = 0.04 \times 0.400$) must be less than $4.2\,\mathrm{GeV} + 0.006 E_{\mathrm{T}}^{\gamma}$. Here E_{T}^{γ} indicates the reconstructed photon transverse energy.

We also require that the shower shape in η, $\sigma_{\eta\eta}$, be consistent with that of a photon. The $\sigma_{\eta\eta}$ variable is a modified second moment of the electromagnetic energy cluster about its mean η position, defined in Ref. [17]. Topological and timing criteria suppress noise present in the ECAL [18]. We reconstruct two photons using the selection described above and require that the invariant mass of the two photons satisfies $M_{\gamma\gamma} > 140$ GeV.

The photon reconstruction and identification efficiency is measured in Monte Carlo (MC) simulation and corrected using a data/MC scale factor of 1.005 ± 0.034 derived from studying $Z \to e^+e^-$ events. The final efficiency is roughly constant as a function of the photon E_{T} and η. The efficiency for an $E_{\mathrm{T}} > 70$ GeV photon with $|\eta| < 1.44$ is $(87.4 \pm 5.4)\%$, where the dominant systematic uncertainty is chosen to cover the variation as a function of the number of reconstructed vertices, photon E_{T}, and photon η. We find that the photon reconstruction efficiency for this analysis depends on the number of extra collisions present in the event only weakly at high photon E_{T}. The corresponding diphoton reconstruction and identification efficiency is $(76.4 \pm 9.6)\%$.

4 Signal Simulation and Optimization

We simulate EDs in the ADD model using version 1.3.0 of the SHERPA [19] MC generator. We simulate several different operating points in M_S and n_{ED}, followed by a fast parametric simulation of the CMS detector [20]. A fast simulation is adequate for describing this multi-photon final state and has been extensively validated using full simulation of the detector via GEANT4 [21]. The simulation includes both SM diphoton production and signal diphoton production via KK-graviton exchange, in order to account for the interference effects. We use the CTEQ6L1 [22] parton distribution functions (PDF) in the simulation. The leading order (LO) SHERPA cross sections are multiplied by a flat next-to-leading order (NLO) K factor of 1.6 ± 0.1. The systematic uncertainty on the signal K factor is introduced to approximate the variation of the K factor as a function of the diphoton mass for a variety of different values of M_S and n_{ED}. It is not intended to account for the theoretical uncertainty. However, a 1.5% relative uncertainty on the signal acceptance is included to account for uncertainty due to the PDF. This K factor represents an updated calculation by the authors of Refs. [23, 24] for 7 TeV pp collisions. The value of the K factor in the previous analysis at CMS [10] was conservatively chosen to be consistent with the Tevatron value.

We note that the LO signal cross section calculations become non-perturbative when the value of $\hat{s}$ in the $2 \to 2$ process exceeds M_S^2. This effect is not taken into account in the SHERPA cross section calculations used in this analysis, so we conservatively assume that the signal cross section is zero for $\sqrt{\hat{s}} > M_S$. The overall effect on the lower limits set in this paper is small, because the values of M_S to which this measurement is sensitive is approaching the kinematic limit of the LHC.

The simulation of the production of RS gravitons is done by the PYTHIA [25] MC program. The simulated signal samples of RS1 gravitons span from $M_1 = 0.25$ to 2.0 TeV in steps of 0.25 TeV, with $\tilde{k}$ =0.01, 0.05, and 0.10. The simulation is reweighted to reflect accurately the number of primary vertices found in the data, thus accounting for the effects of pile-up in the detector. Figure 1 shows the simulated signal shapes for a variety of mass points.

The signal production cross section is scaled by a mass dependent NLO K factor [23, 24], which ranges from 1.6–1.8 as a function of $M_{\gamma\gamma}$ and for different values of $\tilde{k}$. The K factor used for $\tilde{k}$=0.01, 0.05, and 0.10 as a function of the graviton resonance mass is shown in Fig. 2.

The optimization of the event selection is considered separately for both ADD and RS scenarios. The signal in both scenarios is predominantly central while the high $M_{\gamma\gamma}$ SM background is dominant in the forward region; therefore, we restrict ourselves to photons located in the ECAL barrel only.

For the search for EDs in the ADD scenario, the invariant mass selection criterion is optimized to produce the highest expected significance for a potential signal. The significance is computed by calculating the p-value of the background-only hypothesis to equal or exceed the observed number of events in a pseudoexperiment where both the ADD signal and the SM diphoton background are considered. We account for the systematic uncertainty in the background estimate, following the suggestion of Ref. [26]. Pseudoexperiments are generated to compute the expected significance for different luminosity scenarios and ADD model parameters. We find that the $n_{ED} = 2$ case prefers the loosest constraint on $M_{\gamma\gamma}$, and so a requirement of $M_{\gamma\gamma} > 0.8$ TeV for the ADD analysis is chosen. This defines the signal region. The $M_{\gamma\gamma}$ intervals [0.14 TeV, 0.2 TeV], [0.2 TeV, 0.5 TeV], and [0.5 TeV, 0.8 TeV] define the control regions for the ADD analysis.

In the search for RS gravitons, a fixed window is selected about the mass point M_1 of interest.

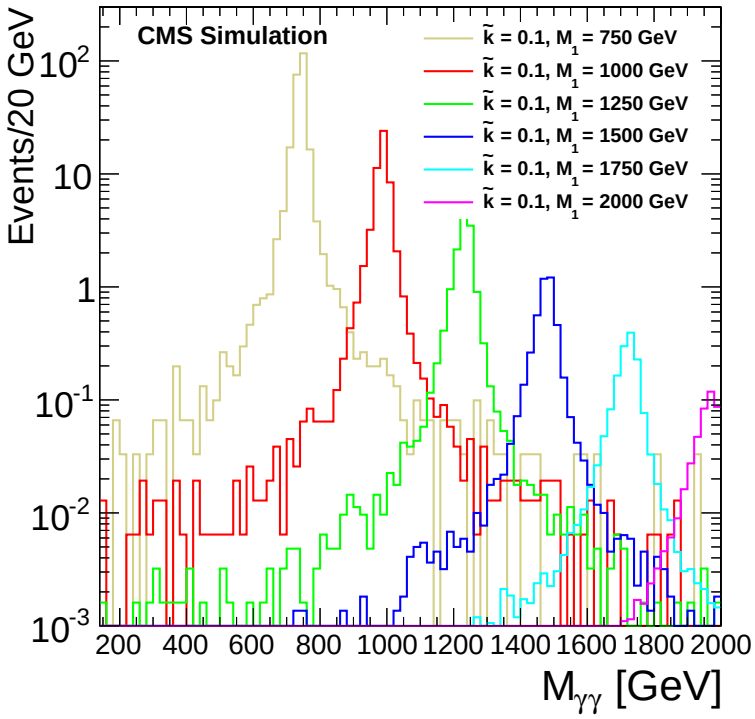

Figure 1: Lineshapes for the RS mass resonances for a variety of mass points with $\tilde{k} = 0.1$.

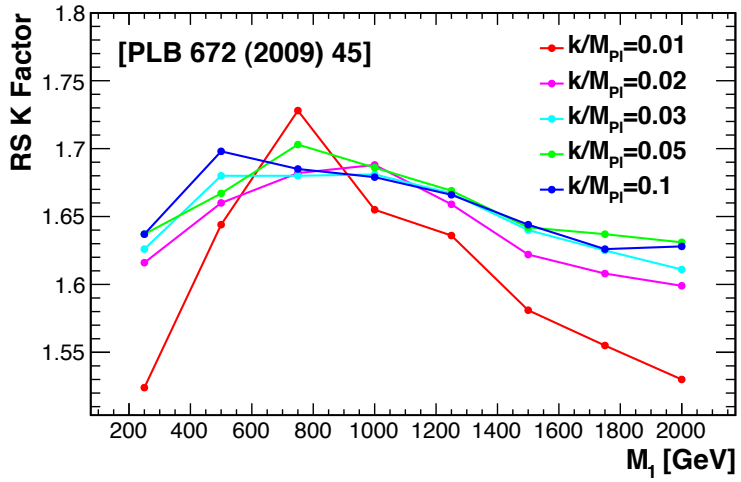

Figure 2: NLO K factors for the RS graviton signal, as a function of resonance mass, for $\tilde{k}$=0.01–0.10. The increase in the K factor with $\tilde{k}$ is due to the increased SM coupling with $\tilde{k}$.

Because the signal shapes deviate from a true Gaussian, we define an effective measure of the signal width σ_{eff} as the half-width of the narrowest mass interval containing 68% of the signal. A window is formed about the resonance mean of size $\pm 5\,\sigma_{\text{eff}}$. This window contains approximately 96–97% of the signal acceptance, for all mass points considered in this analysis. This choice of the window maximizes the signal acceptance and analysis sensitivity in the case of small backgrounds.

5 Background Estimation

Backgrounds due to the mimicking of a photon signal by a jet are small in the signal region but contribute to the control regions. There are two sources of these backgrounds from isolated photon misidentification that we consider: multijet production and prompt photon production (i.e., photons from $\gamma +$ jets). In particular, we measure a misidentification rate, defined as the ratio of the number of isolated photons to non-isolated photons in a sample, where the non-isolated photons are selected similarly to the isolated photons except that they fail one of the isolation or shower-shape criteria. The samples corresponding to numerator and denominator are defined such that they are mutually exclusive. The misidentification rate is measured in a photon triggered sample, but the objects used in the measurement are required to be far away from the triggered object, so as to avoid a trigger-induced bias.

Because the control sample in which we measure the misidentification rate may contain some number of real, isolated photons that "contaminate" the misidentification-rate numerator, we correct for the numerator purity on a sample-by-sample basis. This is done by releasing the $\sigma_{\eta\eta}$ requirement and fitting the numerator sample for the fraction of prompt photons using one-dimensional probability density histograms ("templates") in $\sigma_{\eta\eta}$. The signal template is constructed from MC simulation, and the background template is constructed from reconstructed photons that fail one or more of the isolation criteria. The measured misidentification rate falls from 7% at $E_{\mathrm{T}} = 70$ GeV to 2% at $E_{\mathrm{T}} = 120$ GeV. We apply a conservative 20% systematic uncertainty derived from the variation of the misidentification rate measured in a jet-triggered sample. This is the dominant uncertainty on the background estimation for the dijet and $\gamma +$ jet backgrounds.

The multijet and $\gamma +$ jet backgrounds to the reconstructed diphoton spectrum are estimated by using the misidentification rate to extrapolate from two side-band regions, both selected with the same diphoton trigger as the primary signal sample. One side-band region includes events with only one isolated photon, but one or more non-isolated photons. The other side-band region includes events with no isolated photons, but two or more non-isolated photons. The diphoton trigger is sufficiently inclusive that the side-bands are unaffected by the trigger selection. By applying the prompt-photon misidentification rate to these two side-band regions, we predict the $\gamma +$ jet and multijet backgrounds in the signal region, respectively.

The diphoton background is computed with the PYTHIA MC program and then rescaled by an invariant-mass-dependent NLO K factor. The K factor for this process is computed with the DIPHOX+GAMMA2MC [27, 28] generators and cross-checked with an independent calculation by the authors of Refs. [23, 24]. The DIPHOX generator also takes into account the fragmentation processes in which the photons can come from the collinear fragmentations of hard partons. The photon isolation is calculated inside a cone of $\Delta R < 0.4$, and the hadronic energy inside this cone is required to be less than 5 GeV, a requirement similar to the one imposed at the reconstruction level. The photons are also constrained to have $|\eta| < 1.44$ and $E_{\mathrm{T}} > 70$ GeV at the generator level in the computation of the K factor. The sub-leading-order gluon-fusion Box diagram is included as a part of the LO calculation due to its large contribution at the LHC.

The K factor varies between 1.7–1.1 from low to high $M_{\gamma\gamma}$. The systematic uncertainty on the K factor is estimated by changing the PDF used in DIPHOX+GAMMA2MC from CTEQ6L1 to MSTW08 and by considering the effects of a change in the renormalization, factorization, and fragmentation scales. We observe a maximum of a 15% variation in K factor at high $M_{\gamma\gamma}$, which we take as a systematic uncertainty on the diphoton background.

The simulated diphoton events are reweighted to give the same primary-vertex multiplicity

distribution as in the data and are scaled to account for the differences in photon reconstruction efficiency between data and simulation.

6 Results

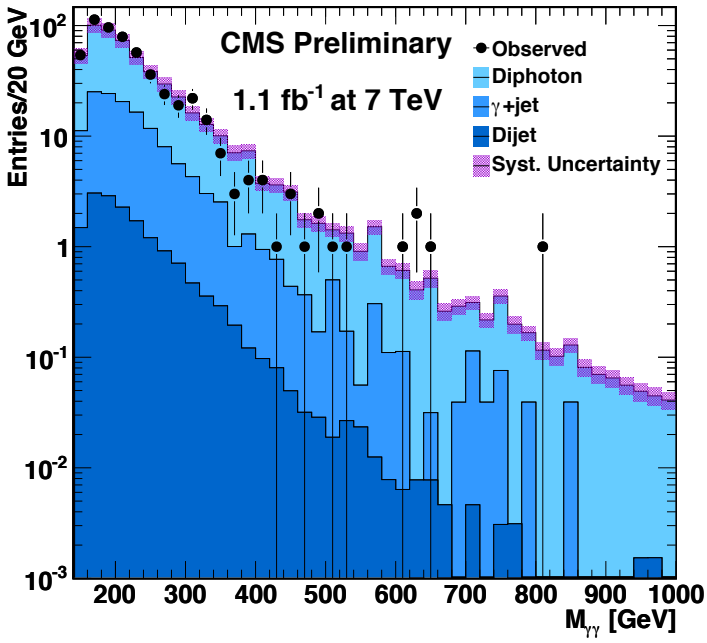

Figure 3: Observed data (points with error bars) and background expectations (filled solid histograms) as a function of the diphoton invariant mass. Photons are required to be isolated, with $E_{\mathrm{T}} > 70$ GeV and $|\eta| < 1.44$. Shaded bands around the background estimation correspond to systematic uncertainties. The last bin is an overflow, including the sum of all contributions for $M_{\gamma\gamma} > 1.2$ TeV.

Figure 3 shows the invariant mass distribution of each of the backgrounds as well as a data distribution. Table 1 presents the data and backgrounds in different reconstructed diphoton invariant mass ranges and corresponds directly to the plot in Fig. 3. The last column corresonds to the signal region. In the control region, we find that the data is consistent with the background estimate within the systematic uncertainty. We do not see any evidence of an excess of events, either resonant or non-resonant.

Table 1: Data measurements and background expectations for reconstructed diphoton invariant mass ranges. Full systematic uncertainties have been included.

Process	Diphoton Invariant Mass Range [TeV]			
	[0.14,0.2]	[0.2,0.5]	[0.5,0.8]	[0.8, ∞)
Multijet	7 $\pm$ 3	9 $\pm$ 3	0.1 $\pm$ 0.1	0.003 $\pm$ 0.001
$\gamma +$ jet	53 $\pm$ 8	67 $\pm$ 10	1.5 $\pm$ 0.2	0.19 $\pm$ 0.04
Diphoton	185 $\pm$ 33	205 $\pm$ 37	7.6 $\pm$ 1.4	1.1 $\pm$ 0.2
Total Backgrounds	245 $\pm$ 35	283 $\pm$ 39	9.2 $\pm$ 1.4	1.3 $\pm$ 0.2
Observed	263	276	6	1

7 Model Limits

In order to set limits on virtual graviton exchange in the ADD scenario, we perform a counting experiment in the signal region ($M_{\gamma\gamma} > 0.8$ TeV) and set 95% CL upper limits on the quantity

$$S \equiv (\sigma_{\text{total}} - \sigma_{\text{SM}}) \times \mathcal{B} \times \mathcal{A}, \tag{8}$$

where σ_{total} represents the total diphoton production cross section (including both signal, SM, and interference effects), and σ_{SM} represents the SM diphoton production cross section. We indicate the signal branching fraction to diphotons by β and the signal acceptance by $\mathcal{A}$. We utilize the CLs technique with Gaussian priors for the nuisance parameters (integrated luminosity, signal efficiency, and background). The likelihood is constructed from the Poisson probability to observe N events, given S, the signal efficiency of $(76.4 \pm 9.6)\%$, the expected number of background events (1.3 ± 0.2), and the integrated luminosity $\mathcal{L} = (1.14 \pm 0.05)$ fb^{-1} [15].

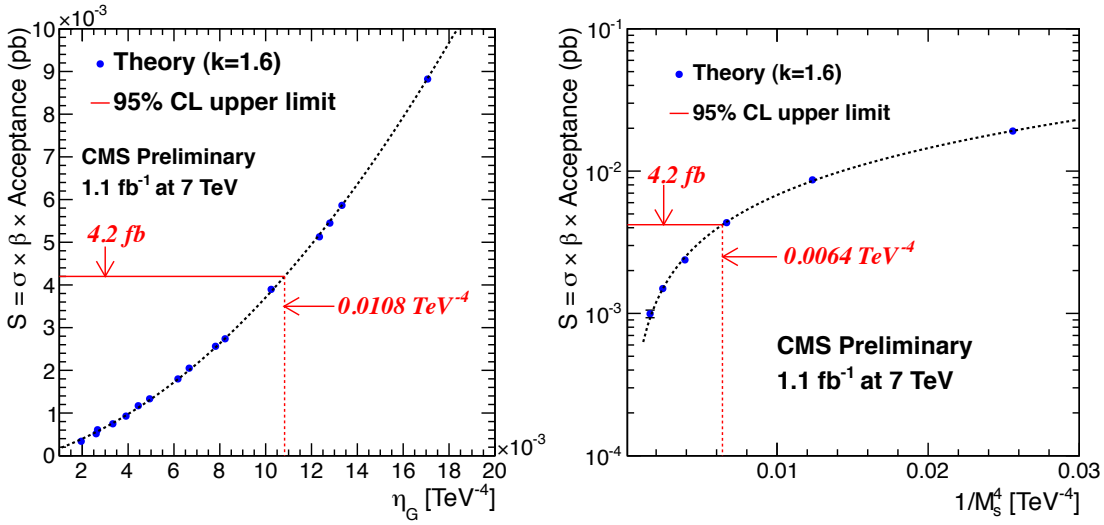

Figure 4: Signal cross section parameterization as a function of the strength of the ED effects, η_G (left) and as a function of $1/M_s^4$ for the $n_{ED} = 2$ case (right).

The observed upper 95% CL limit on S is 4.2 fb. We then translate this limit on the signal into a limit on the parameters of the ADD model, using the following technique. Since the effects of virtual graviton exchange interfere with the SM diphoton production, generally, we expect the overall cross section of the diphoton production from physics sources to have the following form:

$$\sigma_{\text{ADD}} = \sigma_{\text{SM}} + A\eta_G\, \sigma_{\text{int}} + B\eta_G^2\, \sigma_{\text{ED}}, \tag{9}$$

where η_G is the parameter specifying the strength of ED effects. Consequently, we parameterize the signal cross section within the counting window as a bilinear form in the parameter η_G and subtract the σ_{SM} term, already accounted for in setting the cross section limit on the signal. For $n_{\text{ED}} = 2$ case, η_G is not a constant, as it depends on the invariant mass of the diphoton pair. Consequently, in this case we parameterize signal cross section with a smooth function of $1/M_S^4$ and then directly translate the limit on the cross section into the limit on M_S.

The expected 95% CL limit together with the signal cross section parameterization as a function of η_G are shown on the left in Fig. 4. The intersection of the cross section limit with the signal cross section curve determines the upper 95% CL limit on the parameter η_G. As seen from the plot, these limits are equal to $\eta_G = 0.0108$ TeV^{-4} and $1/M_S^4 = 0.0064$ TeV^{-4}. We further translate these limits into the lower limits on the fundamental Planck scale for various numbers

Table 2: Table of 95% CL lower limits on M_S (in TeV), as a function of the number of EDs in the HLZ convention for two different values of the ADD signal K factor. All limits are computed with a signal cross section truncated to zero when $\sqrt{\hat{s}} > M_S$.

K factor	$n_{ED} = 2$	$n_{ED} = 3$	$n_{ED} = 4$	$n_{ED} = 5$	$n_{ED} = 6$	$n_{ED} = 7$
1.0	3.2	3.4	2.8	2.6	2.4	2.2
1.6	3.5	3.7	3.1	2.8	2.6	2.4

of EDs n_{ED}, as shown in Table 2. This is calculated trivially for $n_{ED} = 2$ and for $n_{ED} > 2$ by using Eq. (6).

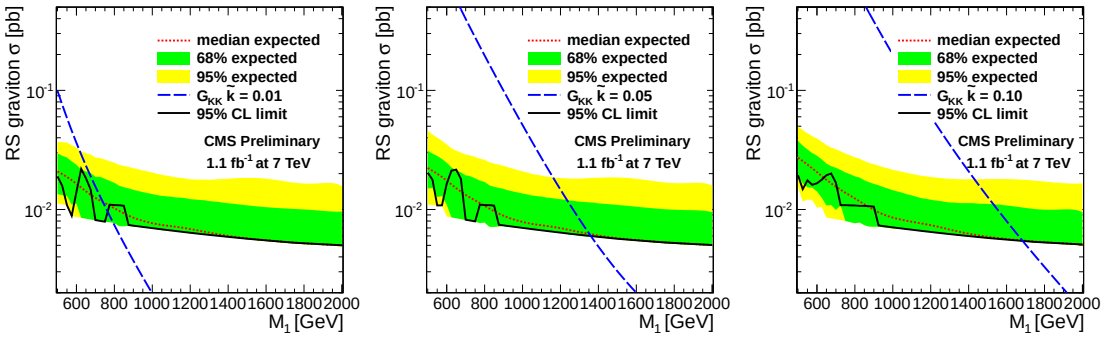

Figure 5: Observed and expected limits on the Kaluza–Klein graviton (G_{KK}) mass M_1 for $\tilde{k} = 0.01$ (top left), $\tilde{k} = 0.05$ (top right), and $\tilde{k} = 0.10$ (bottom). The theoretical cross section for the G_{KK} is given by the dashed blue line.

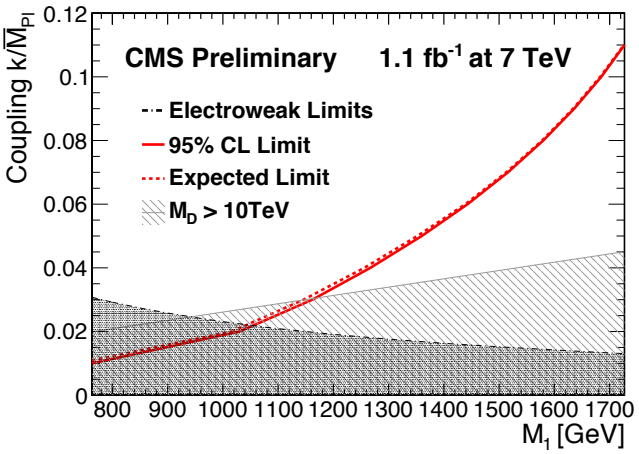

Figure 6: The 95% CL lower limits on the RS1 graviton model in the M_1–$\tilde{k}$ plane. Also shown are bounds due to electroweak constraints [29] and naturalness ($M_D > 10$ TeV) are shown. All points in the plane above and to the left of the red line have been excluded by the measurement presented in this paper. Perturbativity requirements bound $\tilde{k} \lesssim 0.10$.

For the RS scenario, we perform a similar limit setting procedure, but in a bounded window in $M_{\gamma\gamma}$, as described in Sec. 4. The results are given as a ratio of the excluded cross section to the RS signal model cross section, including the mass dependent K factor. The corresponding limit in terms of M_1 is found when the two quantities are equal. For the values of $\tilde{k}$ and M_1 that were not simulated, we have interpolated the theory cross section, signal yield, and signal width. We then use the interpolated signal width to set the corresponding counting window for the background yield.

Table 3: Table of 95% CL lower limits on M_1 for given values of the coupling parameter, $\tilde{k}$.

$\tilde{k}$	0.01	0.02	0.03	0.04	0.05	0.06	0.07	0.08	0.09	0.10	0.11
M_1 [TeV]	0.77	1.05	1.20	1.31	1.41	1.49	1.57	1.63	1.69	1.74	1.78

Table 4: Expected signal and background yields given model parameters $\tilde{k}$ and M_1 in predefined bounded mass ranges in $M_{\gamma\gamma}$. Shown additionally are the observed number of events and observed and expected 95% CL upper limit on the production cross section times acceptance times branching fraction in the given mass range.

$\tilde{k}$	M_1 [GeV]	Mass Window [GeV]	Signal Efficiency	Expected Background	Observed
0.01	500	470–530	0.29	4.3	4
0.01	750	707–793	0.34	1.1	0
0.01	1000	945–1055	0.38	0.2	0
0.01	1250	1182–1318	0.43	0.1	0
0.01	1500	1420–1580	0.47	0.03	0
0.01	1750	1657–1843	0.51	0.01	0
0.01	2000	1895–2105	0.53	0.007	0
0.05	500	464–536	0.28	5.4	5
0.05	750	698–802	0.34	1.3	0
0.05	1000	933–1067	0.38	0.3	0
0.05	1250	1167–1333	0.43	0.2	0
0.05	1500	1402–1598	0.47	0.03	0
0.05	1750	1636–1864	0.51	0.01	0
0.05	2000	1871–2129	0.53	0.007	0
0.010	500	444–556	0.28	9.9	7
0.010	750	669–831	0.33	1.9	1
0.010	1000	894–1106	0.38	0.4	0
0.010	1250	1118–1382	0.42	0.3	0
0.010	1500	1343–1657	0.46	0.05	0
0.010	1750	1568–1932	0.50	0.02	0
0.010	2000	1793–2207	0.52	0.01	0

Figure 6 shows the excluded regions of the M_1–$\tilde{k}$ plane. Bounds due to precision electroweak measurements [29] as well as due to naturalness arguments (when the fundamental Planck scale exceeds 10 TeV) are shown. Table 3 presents the 95% CL lower limits on the graviton mass M_1 for different values of $\tilde{k}$. Table 4 summarizes the expected background, signal efficiency, and observed number of events for different mass windows, corresponding to particular choices of RS model parameters. Figure 5 shows the observed and expected limits as a function of the graviton mass for $\tilde{k}$ =0.01, 0.05, and 0.10, respectively. All mass points for which the solid black line lies below the blue theory line are excluded.

8 Conclusions

We have performed a search for large extra spatial dimensions leading to enhanced diphoton production in proton-proton collisions at a center of mass energy 7 TeV at the LHC. Using 1.1 fb^{-1} of integrated luminosity recorded by the CMS experiment, we observe no excess in

diphoton production above that predicted from SM background sources. We present limits on both the ADD and RS1 model of extra dimensions in the diphoton final state that extend those achieved at the Tevatron [12] as well as those set previously by the CMS experiment [10]. Values of the cutoff scale M_S less than 2.2–3.6 TeV are excluded at 95% CL for ADD models with between 2–7 extra dimenions. We also exclude at 95% CL resonant graviton production in the RS1 model with values of M_1 less than 0.76–1.72 TeV depending on the normalized coupling strength, $\tilde{k}$. These are the most stringent limits on these models set to date at a particle collider.

References

[1] E. Witten, "Mass Hierarchies in Supersymmetric Theories", *Phys. Lett. B* **105** (1981) 267. doi:10.1016/0370-2693(81)90885-6.

[2] N. Arkani-Hamed, S. Dimopoulos, and G. Dvali, "The Hierarchy Problem and New Dimensions at a Millimeter", *Phys. Lett. B* **429** (1998) 263.

[3] N. Arkani-Hamed, S. Dimopoulos, and G. Dvali, "Phenomenology, astrophysics and cosmology of theories with submillimeter dimensions and TeV scale quantum gravity", *Phys. Rev.* **D59** (1999) 086004, arXiv:hep-ph/9807344. doi:10.1103/PhysRevD.59.086004.

[4] L. Randall and R. Sundrum, "A large mass hierarchy from a small extra dimension", *Phys. Rev. Lett.* **83** (1999) 3370–3373, arXiv:hep-ph/9905221. doi:10.1103/PhysRevLett.83.3370.

[5] G. Giudice, R. Rattazzi, and J. Wells, "Quantum Gravity and Extra Dimensions at High-Energy Colliders", *Nucl. Phys. B* **544** (1999) 3.

[6] T. Han, J. Lykken, and R.-J. Zhang, "Kaluza–Klein states from large extra dimensions", *Phys. Rev. D* **59** (1999) 105006.

[7] J. Hewett, "Indirect Collider Signals for Extra Dimensions", *Phys. Rev. Lett.* **82** (1999) 4765.

[8] Particle Data Group Collaboration, "The Review of Particle Physics", *J. Phys.* **G37** (2010) 075021. doi:10.1088/0954-3899/37/7A/075021.

[9] K. Cheung and G. Landsberg, "Kaluza–Klein states of the standard model gauge bosons: Constraints from high energy experiments", *Phys. Rev. D* **62** (2000) 076003.

[10] CMS Collaboration, "Search for Large Extra Dimensions in the Diphoton Final State at the Large Hadron Collider", *JHEP* **1105** (2011) 085, arXiv:1103.4279.

[11] D0 Collaboration, "Measurement of dijet angular distributions at sqrts=1.96TeV and searches for quark compositeness and extra spatial dimensions", *Phys. Rev. Lett.* **103** (2009) 191803, arXiv:0906.4819. doi:10.1103/PhysRevLett.103.191803.

[12] D0 Collaboration, "Search for Large extra spatial dimensions in the dielectron and diphoton channels in $p\bar{p}$ collisions at $\sqrt{s}$ =1.96 TeV", *Phys. Rev. Lett.* **102** (2009) 051601, arXiv:0809.2813. doi:10.1103/PhysRevLett.102.051601.

[13] The D0 Collaboration, "Search for Randall-Sundrum gravitons in the dielectron and diphoton final states with 5.4 fb-1 of data from ppbar collisions at sqrt(s)=1.96 TeV", *Phys. Rev. Lett.* **104** (2010) 241802, arXiv:1004.1826. doi:10.1103/PhysRevLett.104.241802.

[14] CMS Collaboration, "The CMS experiment at the CERN LHC", *JINST* **3** (2008) S08004. doi:10.1088/1748-0221/3/08/S08004.

[15] CMS Collaboration, "Measurement of CMS Luminosity", CMS PAS EWK-10-004.

[16] CMS Collaboration, "CMS tracking performance results from early LHC Operation", *Eur.Phys.J.C* **70** (2010) 1165–1192, arXiv:1007.1988. doi:10.1140/epjc/s10052-010-1491-3.

[17] CMS Collaboration, "Measurement of isolated photon production cross section in pp collisions at sqrt(s)=7 TeV", *Phys. Rev. Lett.* **106** (2011) 082001, arXiv:1012.0799. doi:10.1103/PhysRevLett.106.082001.

[18] CMS Collaboration, "Isolated Photon Reconstruction and Identification at $\sqrt{(}s) = 7$ TeV", *CMS Physics Analysis Summary* **2010/006** (2010).

[19] T. Gleisberg et al., "SHERPA 1.α, a proof-of-concept version", *JHEP* **02** (2004) 056.

[20] D. Orbaker, "Fast Simulation of the CMS Detector", *J. Phys. Conf. Ser.* **219** (2010) 032053. doi:10.1088/1742-6596/219/3/032053.

[21] GEANT 4 Collaboration, "GEANT4 – a simulation toolkit", *Nucl. Instr. and Methods* **A506** (2003) 250. doi:10.1016/S0168-9002(03)01368-8.

[22] CTEQ Collaboration, "Implications of CTEQ global analysis for collider observables", *Phys. Rev.* **D78** (2008) 013004, arXiv:0802.0007. doi:10.1103/PhysRevD.78.013004.

[23] M. Kumar, P. Mathews, V. Ravindran et al., "Diphoton signals in theories with large extra dimensions to NLO QCD at hadron colliders", *Phys. Lett. B* **672** (2009) 45.

[24] M. Kumar, P. Mathews, V. Ravindran et al., "Direct photon pair production at the LHC to order α_s in TeV scale gravity models", *Preprint arXiv:0902.4894 [hep-ph]* (2009).

[25] T. Sjostrand, P. Eden, C. Friberg et al., "High-Energy-Physics Event Generation with PYTHIA 6.1", 2000.

[26] R. D. Cousins, J. T. Linnemann, and J. Tucker, "Evaluation of three methods for calculating statistical significance when incorporating a systematic uncertainty into a test of the background-only hypothesis for a Poisson process", arXiv:physics/0702156.

[27] T. B. et al., "A Full next-to-leading order study of direct photon pair production in hadronic collisions", *Eur. Phys. J.* **C16** (2000) 311.

[28] Z. Bern, L. Dixon, and C. Schmidt, "Isolating a light Higgs boson from the diphoton background at the LHC", *Phys. Rev.* **D66** (2002) 074018.

[29] H. Davoudiasl, J. L. Hewett, and T. G. Rizzo, "Experimental probes of localized gravity: On and off the wall", *Phys. Rev.* **D63** (2001) 075004, arXiv:hep-ph/0006041. doi:10.1103/PhysRevD.63.075004.